

Atomically Thin CrCl₃: An in-Plane Layered Antiferromagnetic Insulator

Xinghan Cai,^{1,2} Tiancheng Song,¹ Nathan P. Wilson,¹ Genevieve Clark,³ Minhao He,¹ Xiaou Zhang,⁴ Takashi Taniguchi,⁵ Kenji Watanabe,⁵ Wang Yao,⁶ Di Xiao,⁴ Michael A. McGuire,⁷ David H. Cobden,¹ Xiaodong Xu^{1,3*}

¹Department of Physics, University of Washington, Seattle, Washington 98195, USA.

²National Key Laboratory of Science and Technology on Micro/Nano Fabrication, Department of Micro/Nano Electronics, Shanghai Jiao Tong University, Shanghai 200240, China.

³Department of Materials Science and Engineering, University of Washington, Seattle, Washington 98195, USA.

⁴Department of Physics, Carnegie Mellon University, Pittsburgh, Pennsylvania 15213, USA.

⁵National Institute for Materials Science, Tsukuba, Ibaraki 305-0044, Japan.

⁶Department of Physics and Center of Theoretical and Computational Physics, University of Hong Kong, Hong Kong, China.

⁷Materials Science and Technology Division, Oak Ridge National Laboratory, Oak Ridge, Tennessee 37831, USA.

*Correspondence to: xuxd@uw.edu

Abstract: The recent discovery of magnetism in atomically thin layers of van der Waals (vdW) crystals has created new opportunities for exploring magnetic phenomena in the two-dimensional (2D) limit. In most 2D magnets studied to date the c-axis is an easy axis, so that at zero applied field the polarization of each layer is perpendicular to the plane. Here, we demonstrate that atomically thin CrCl₃ is a layered antiferromagnetic insulator with an easy-plane normal to the c-axis, that is the polarization is in the plane of each layer and has no preferred direction within it. Ligand field photoluminescence at 870 nm is observed down to the monolayer limit, demonstrating its insulating properties. We investigate the in-plane magnetic order using tunneling magnetoresistance in graphene/CrCl₃/graphene tunnel junctions, establishing that the interlayer coupling is antiferromagnetic down to the bilayer. From the temperature dependence of the magnetoresistance we obtain an effective magnetic phase diagram for the bilayer. Our result shows that CrCl₃ should be useful for studying the physics of 2D phase transitions and for making new kinds of vdW spintronic devices.

Keywords: 2D magnetic insulator, in-plane layered antiferromagnetism, magnetic tunnel junction, weak magnetic anisotropy, magnetic phase transition

The experimental observation of magnetism in atomically thin films¹⁻⁸ has opened a new avenue to study novel magnetic multilayered devices using 2D materials⁹⁻²¹. To date, all magnetic compounds that have been successfully synthesized down to the monolayer limit exhibit strong Ising anisotropy, which supports an out-of-plane magnetization within each layer. In this regard,

CrCl₃ represents a curious case in that bulk CrCl₃ is known to be a weakly coupled, layered antiferromagnet with small XY anisotropy (Figure 1a)²²⁻²⁵. Therefore, exfoliating CrCl₃ offers the intriguing possibility to realize a strictly 2D magnetic insulator with in-plane magnetization. This could be useful for investigating how a magnet with weak anisotropy evolves on approaching the 2D limit. The monolayer may behave as a good approximation to the 2D XY-model, analogous to thin film superfluids, superconductors and liquid crystals^{26,27}, allowing the study of the Berezinskii–Kosterlitz–Thouless (BKT) transition²⁸ and related phenomena. Moreover, the in-plane magnetization is also complementary to the out-of-plane magnetization in terms of the proximity effect²⁹⁻³³ when CrCl₃ is layered with other 2D materials.

CrCl₃ flakes were exfoliated onto SiO₂/Si substrates. In atomic force microscope images (Figure 1b), bilayers and trilayer regions appear 1.2 nm and 1.8 nm thick, respectively, consistent with a previous report²⁵. Figure 1c shows both the circular polarization components of the photoluminescence (PL) from a ~ 5 nm thick sample at a temperature of 2 K, well below the Neel temperature of ~ 14 K. The excitation laser is 20 μW, linearly polarized, and at 532 nm. A single broad peak centered at ~ 870 nm is seen, analogous to the parity-forbidden *d-d* ligand-field transition in CrI₃³⁴. Unlike in CrI₃, however, the two polarization components are indistinguishable, indicating that there is no out-of-plane magnetization component in CrCl₃. This PL emission feature persists down to the monolayer CrCl₃ (Figure 1d), implying that the insulating nature retains in CrCl₃ to its 2D limit.

To investigate the in-plane magnetization we employ vertical tunneling measurements, which are sensitive to the relative alignment of spins in different layers. As sketched in Figure 2a, a few layer CrCl₃ tunnel barrier is sandwiched between top and bottom thin graphite flakes to form magnetic tunnel junction (MTJ), this being further encapsulated in hexagonal boron nitride (h-BN) to avoid degradation (see Methods). Figure 2b shows the tunneling current, I_t , as a function of DC bias voltage, V , measured at 2 K for a bilayer CrCl₃ device whose optical image is inset. With an applied in-plane magnetic field $\mu_0 H_{in} = 2$ T (red trace) the current is enhanced relative to its value at zero field (blue trace), implying a change in the spin configuration of the CrCl₃³⁵. The bottom inset shows the tunneling magnetoresistance (TMR), defined as $100\% \times [I_t(2 \text{ T}) - I_t(0)]/I_t(0)$ ¹³. The TMR is largest at low bias, where the response is linear. Figure 2c shows the tunneling current, I_t , here measured using a small AC bias of $V_{ac} = 1$ mV, as a function of magnetic field. For either in-plane field (H_{in} , orange) or out-of-plane field (H_{out} , green), I_t increases smoothly before plateauing out when the field exceeds a critical value ($\mu_0 H_{in}^c = 1.2$ T and $\mu_0 H_{out}^c = 1.5$ T). This behavior is similar to that seen for an in-plane field in CrI₃ MTJs. It implies that the spin polarizations of the two layers are opposite at zero field, suppressing the tunneling current by a spin-filtering effect, but become increasingly aligned due to the Zeeman term in an external field. This in turn suggests that the layered antiferromagnetic order of the bulk crystal, with in-plane ferromagnetic polarization that alternates in direction between adjacent layers, persists in the bilayer limit.

The fact that H_{out}^c is only slightly larger than H_{in}^c , and the smooth rise of I_t seen for both field orientations, are consistent with relatively weak anisotropy in the material. Indeed, the field

dependence of the tunneling current can be well fit by a simple model of two antiferromagnetically coupled macrospins with easy-plane anisotropy,

$$H = J_{AF} \mathbf{s}_1 \cdot \mathbf{s}_2 + \frac{K}{2} (s_{1,z}^2 + s_{2,z}^2) - g\mu_B \mathbf{B} \cdot (\mathbf{s}_1 + \mathbf{s}_2),$$

where $J_{AF} > 0$ is the interlayer antiferromagnetic exchange, $K > 0$ is the easy-plane anisotropy energy, and \mathbf{B} is the magnetic field. According to our fitting, the anisotropy is $KS/g\mu_B = 0.27$ T and interlayer coupling is $J_{AF}S/g\mu_B = 0.6$ T (See Supplementary material). We note that there is some asymmetry of I_t as a function of H_{in} , associated with hysteresis as shown in Figure 2d. This might be due to a spin-flop transition associated with a previously reported, very small easy-axis anisotropy (10 Oe) within the easy-plane^{24,25}. No hysteresis is seen as a function of H_{out} (Figure 2d, inset), as expected for spin canting in a magnetic field perpendicular to the zero-field polarization. This is in sharp contrast to the situation in bilayer CrI_3 , where the transition from antiferromagnetic to a fully aligned ferromagnetic state in a perpendicular field is a sudden spin-flip transition.

The picture of layered antiferromagnetism is further supported by measurements on a trilayer CrCl_3 MTJ device (Figure 3), an optical micrograph of which is inset to Figure 3b. The thicker barrier presented by a trilayer leads to much weaker tunneling which necessitates a much larger DC bias of 600 mV to achieve a suitable signal to noise ratio. As seen in Figure 3a, I_t increases smoothly with H_{out} , again consistent with gradual spin canting out of the layers as in the bilayer case¹³. However, as a function of H_{in} the current exhibits a plateau near zero field below a critical value, above which it smoothly rises and reaches a plateau when the magnetic field is large enough to align all three layers to the fully spin polarized state.

To test for magnetic anisotropy within the plane of the layers, we measured the tunneling current while varying the orientation, θ , of H_{in} within the plane. Figure 3b shows I_t as a function of H_{in} at selected angles, while Figure 3c is a polar plot of I_t as a function of angle at selected magnetic fields. No significant dependence on θ is observed, implying that the overall magnetic order can rotate freely about the c-axis, i.e., the plane of the layers is an easy plane. The observed plateau of tunneling current as a function of in-plane magnetic field is due to the uncompensated total magnetization in a trilayer, consistent with the picture of layered antiferromagnetism. We conclude that atomically thin CrCl_3 can be well described as a layered antiferromagnetic insulator with easy-plane magnetic anisotropy.

Figure 4a shows the tunneling current I_t measured AC with $V_{ac} = 5$ mV as a function of T at selected in-plane magnetic fields. At $H_{in} = 0$, on increasing T from base, at first I_t increases. This can be explained by suppression of the spin filtering effect due to thermal fluctuations which reduce the degree of antiferromagnetic alignment between the layers. Then, above a peak at the intralayer ferromagnetic critical temperature $T \sim 17$ K, I_t starts to decrease. This suggests that ferromagnetic order within each layer assists coherent tunneling, and rising temperature suppresses this order. At still higher temperatures I_t increases again, as expected since once no magnetic order remains the tunneling rate should simply be activated. When an in-plane field is applied it competes with the antiferromagnetic alignment and reduces the temperature at which the AFM order appears, so the

peak moves to lower T . It also increases net spin alignment above the critical temperature and so increases the current. For $\mu_0 H_{in} > 1.2$ T, the antiferromagnetism is completely suppressed and the spins are fully polarized at base temperature.

The results in Figure 4a can be presented in a more visualized way: dI_t/dT has been plotted as a function of the temperature at selected $\mu_0 H_{in}$ (Figure 4b). In the top panel, dI_t/dT clearly exhibits two times of the sign flip as T increases. This is similar to what has been reported in CrCl_3 3D bulk crystal²⁵, which is interpreted as a two-step phase transition, i.e. from the layered antiferromagnetic phase to the ferromagnetic phase (first transition) and eventually to the paramagnetic phase (second transition) as T increases. Here we assign the peak (directed by the green arrow) in each curve to the critical temperature of the first transition and the dip (directed by the blue arrow) to the second one. For magnetic fields higher than 1.2 T, as shown in the bottom panel, no local maximum shows up, thus only T_c for the second transition is determined. In Figure 4c, we present the 2D semi-log plot of the normalized dI_t/dT as a function of both $\mu_0 H_{in}$ and T (see supplementary material for the plot without the normalization of dI_t/dT). This plot, though not a legitimate phase diagram, facilitates comparison with the phase diagram of the 3D bulk crystal in which distinct transitions are identified between the layered AFM phase, a fully spin-polarized phase, and paramagnetic phase²⁵.

To recap, we find that the van der Waals magnetic insulator CrCl_3 shows layered antiferromagnetism down to the bilayer limit with the magnetic moments in the plane of the layers and little or no anisotropy within the plane. CrCl_3 thus provides a new model system for studying 2D in-plane magnetism and its proximate coupling to other 2D materials, such as 2D superconductors, topological insulators, and stacked heterostructures^{30,36} for potential use in novel magneto-electronic devices¹³⁻¹⁸.

During the final preparation of the manuscript, we became aware of the two relevant works posted on ArXiv^{37,38}.

METHODS

Device fabrication: V/Au (4 nm/40 nm) metal electrodes were deposited on a 90 nm SiO_2/Si substrate in the vicinity of the exfoliated h-BN thin flake (bottom h-BN), following the standard e-beam lithography procedures. Bulk CrCl_3 crystals were grown by chemical vapour transport, as described in detail in ref²⁵. Few layer CrCl_3 , cleaved from these crystals in an inert gas glovebox with oxygen and water levels below 1 ppm, was stacked between the pre-exfoliated top h-BN/graphite and bottom graphite and transferred onto the bottom h-BN using a polymer-based dry transfer technique³⁹. Top/bottom graphite flakes were contacted by the pre-patterned metal electrodes and the tunnel junction was then fully encapsulated before finally dissolving the polymer in chloroform outside the glovebox. The thickness of the h-BN (5-35 nm) and graphite (2-8 nm) were determined by atomic force microscopy, while the number of layers of CrCl_3 was identified from the optical contrast.

Optical measurements: Low-temperature magneto-PL measurements were performed in a closed-cycle cryostat with a superconducting magnet with field normal to the sample. The sample was excited by a continuous-wave laser (633 nm or 532 nm) with the power below 50 μW to avoid

sample heating and degradation. The PL signal was detected by a silicon CCD array and the excitation and detection polarization were controlled using linear polarizers and half- and quarter-wave plates.

Electrical measurements: All magneto-transport measurements were carried out in a PPMS DynaCool cryostat (Quantum Design, Inc) with a base temperature of 1.8 K and magnetic field up to 9 T. The CrCl_3 MTJ devices were mounted in a Horizontal Rotator probe using either a Rotator Universal Sample Board (P103C), which allows rotations about an axis in the sample plane perpendicular to the magnetic field, or a Rotator Field Parallel Sample Board (P103D) for rotation about the magnetic field axis. The bias voltage is applied to the top graphite contact while the current from the bottom graphite contact is measured using a virtual-earth current preamplifier (DL Instruments; Model 1211). AC measurements were made using a lock-in amplifier (Stanford Research 830) at 13.7 Hz.

Figure Captions:

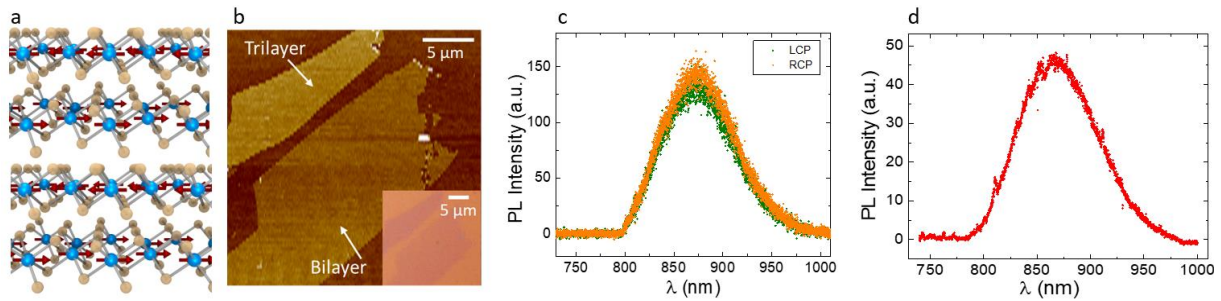


Figure 1. CrCl_3 crystal structure and the optical characterization. (a) Side view of the structure of CrCl_3 . The colored balls represent Cr (blue) and Cl (grey), respectively. Red arrows indicate the magnetization. (b) Atomic force micrograph of few layer CrCl_3 flakes. The inset is an optical micrograph of the same area. (c) Left and right circular polarization components of photoluminescence from a 5 nm thick flake under a linearly polarized excitation at 532 nm. (d) Photoluminescence spectrum of a monolayer CrCl_3 .

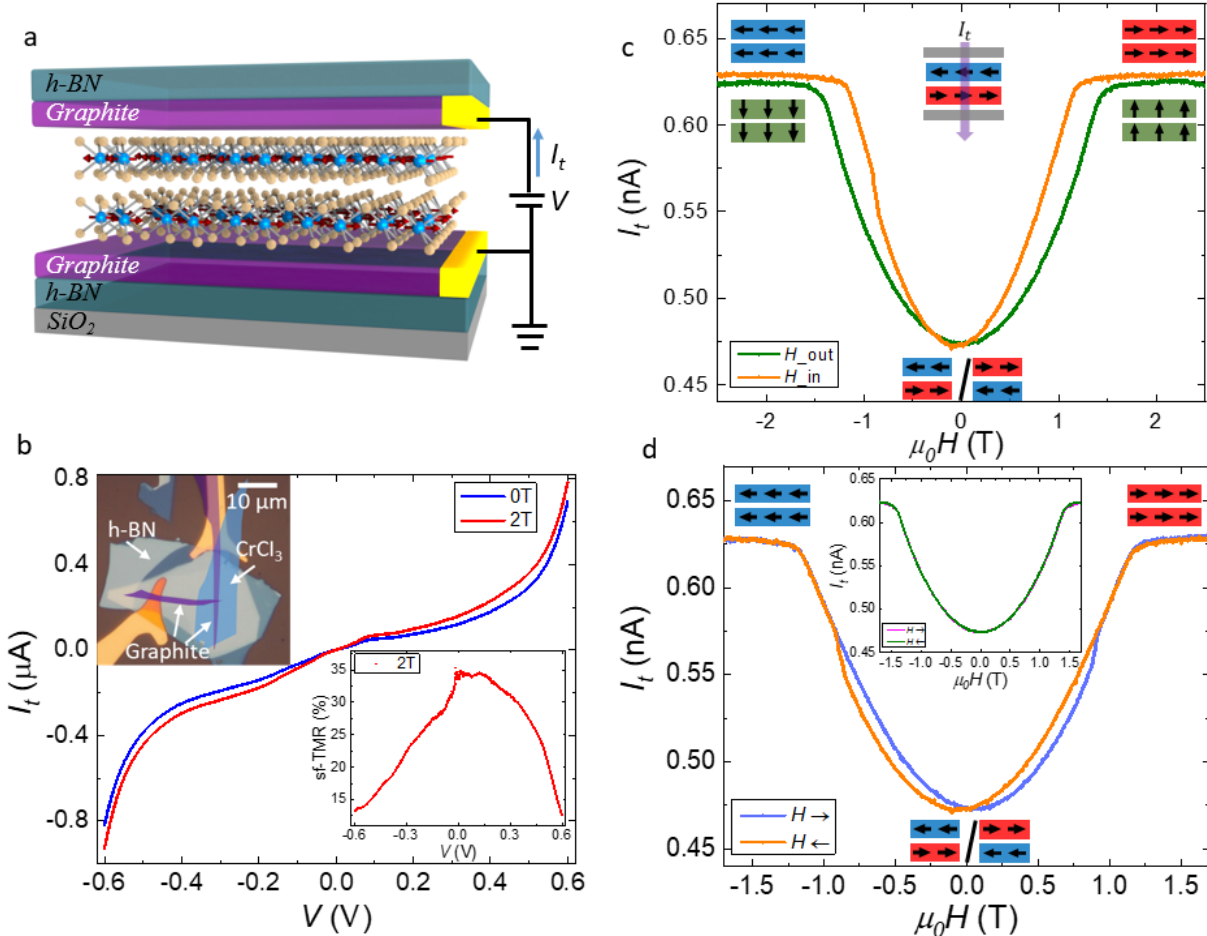


Figure 2. Magnetic field dependent tunneling in a bilayer CrCl₃ spin-filter magnetic tunnel junction (sf-MTJ). (a) Schematic of device with graphite contacts encapsulated by h-BN. (b) Tunneling current as a function of the DC bias voltage with (red) and without (blue) an in-plane magnetic field $\mu_0 H_{in} = 2$ T. Top inset: optical microscope image of the device with false coloring for clarity. Bottom inset: TMR ratio. (c) Tunneling current I_t as a function of in-plane (orange) and out-of-plane (green) magnetic field for bias $V_{ac} = 1$ mV. The corresponding magnetic states are indicated. (d) Tunneling current vs in-plane magnetic field sweep in both directions. The magnetic configurations are indicated. Top inset: Tunneling current vs out-of-plane field swept in both directions, showing no hysteresis.

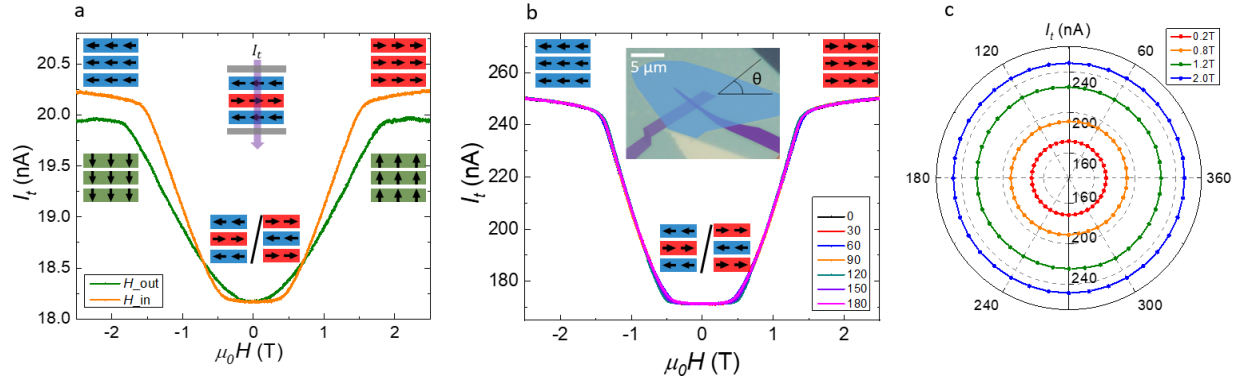


Figure 3. Magnetic field dependent tunneling in a tri-layer CrCl_3 sf-MTJ device. (a) Tunneling current I_t as a function of the in-plane (orange) and out-of-plane (green) magnetic field at $V_{dc} = 600$ mV. The corresponding magnetic states are indicated. (b) Tunneling current as a function of in-plane magnetic field at selected orientations θ (here $V_{dc} = 750$ mV). The inset is a false-color optical micrograph of the device with θ defined. (c) Polar plot of the tunneling current as a function of θ at selected magnetic fields.

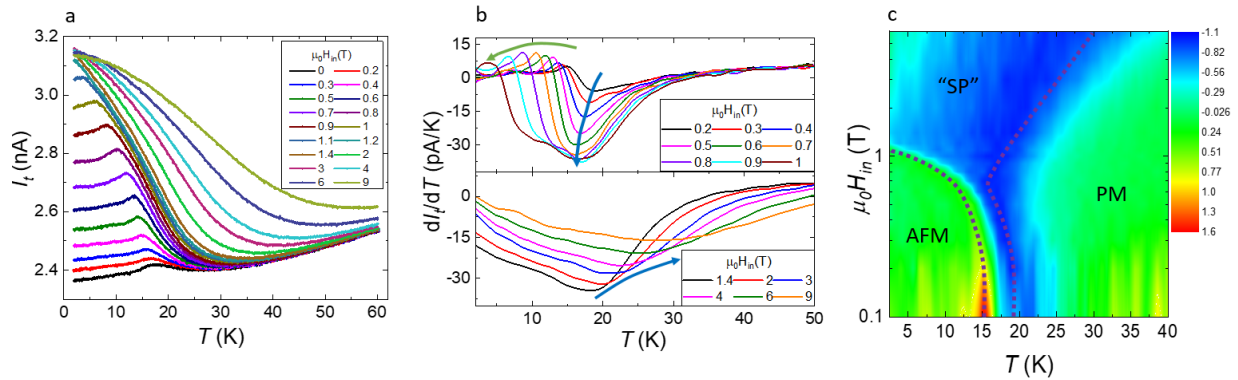


Figure 4. Temperature dependent tunneling and the magnetic phase diagram of bilayer CrCl_3 . (a) Tunneling current I_t as a function of the temperature at selected in-plane magnetic fields with the AC bias voltage $V_{ac} = 5$ mV. (b) The derivative of the tunneling current to the temperature at low (top panel) and high (bottom panel) in-plane magnetic fields. The green/blue arrows indicate the critical temperature of the transition from layered antiferromagnetic/spin polarized to spin polarized/paramagnetic states, respectively. (c) Color plot of normalized dI_t/dT as a function of in-plane magnetic field H_{in} and temperature T . AFM: Layered antiferromagnetic. PM: Paramagnetic. SP: Fully spin polarized.

Acknowledgements: Funding: The work at UW is mainly supported by NSF MRSEC 1719797. Device fabrication and transport measurements are partially supported by NSF-DMR-1708419. Photoluminescence measurement is supported by DOE BES DE-SC0012509. Work at HKU is supported by the Croucher Foundation (Croucher Innovation Award), RGC of HKSAR (17303518P). Work at ORNL (M.A.M.) was supported by the US Department of Energy, Office of Science, Basic Energy Sciences, Materials Sciences and Engineering Division. K.W. and T.T. acknowledge support from the Elemental Strategy Initiative conducted by the MEXT, Japan, A3 Foresight by JSPS and the CREST(JPMJCR15F3), JST. D.X. acknowledges the support of a Cottrell Scholar Award. X.X. acknowledges the support from the State of Washington funded Clean Energy Institute and from the Boeing Distinguished Professorship in Physics.

Author Contributions: X.X., X.C., M.A.M. conceived the project. X.C. fabricated the devices, performed the experiments, and analyzed the data, assisted by T.S. and M.H. N.P.W. and G.C. performed photoluminescence measurements. X.Z. analyzed the macrospin model and the tunneling current dependence on the magnetic structure. X.X., D.X., W.Y., and D.H.C. supervised the project. M.A.M. provided and characterized bulk CrCl₃ crystals. T.T. and K.W. provided and characterized bulk hBN crystals. X.C., X.X., D.H.C. and D.X. wrote the manuscript with input from all authors.

Competing Financial Interests: The authors declare no competing financial interests.

Data Availability: The data that support the findings of this study are available from the corresponding author upon reasonable request.

REFERENCES

1. Huang, B. et al. Layer-dependent ferromagnetism in a van der Waals crystal down to the monolayer limit. *Nature* **546**, 270 (2017).
2. Gong, C. et al. Discovery of intrinsic ferromagnetism in two-dimensional van der Waals crystals. *Nature* **546**, 265 (2017).
3. Ghazaryan, D. et al. Magnon-assisted tunnelling in van der Waals heterostructures based on CrBr₃. *Nature Electronics* **1**, 344-349 (2018).
4. Lin, M.-W. et al. Ultrathin nanosheets of CrSiTe₃: a semiconducting two-dimensional ferromagnetic material. *Journal of Materials Chemistry C* **4**, 315-322 (2016).
5. Yao, T., Mason, J.G., Huiwen, J., Cava, R.J. & Kenneth, S.B. Magneto-elastic coupling in a potential ferromagnetic 2D atomic crystal. *2D Materials* **3**, 025035 (2016).
6. McGuire, M.A., Dixit, H., Cooper, V.R. & Sales, B.C. Coupling of Crystal Structure and Magnetism in the Layered, Ferromagnetic Insulator CrI₃. *Chemistry of Materials* **27**, 612-620 (2015).
7. Bonilla, M. et al. Strong room-temperature ferromagnetism in VSe₂ monolayers on van der Waals substrates. *Nature Nanotechnology* **13**, 289-293 (2018).
8. Tan, C. et al. Hard magnetic properties in nanoflake van der Waals Fe₃GeTe₂. *Nature Communications* **9**, 1554 (2018).
9. Novoselov, K.S., Mishchenko, A., Carvalho, A. & Castro Neto, A.H. 2D materials and van der Waals heterostructures. *Science* **353**, aac9439 (2016).
10. Yuasa, S., Nagahama, T., Fukushima, A., Suzuki, Y. & Ando, K. Giant room-temperature magnetoresistance in single-crystal Fe/MgO/Fe magnetic tunnel junctions. *Nature Materials* **3**, 868 (2004).

11. Lee, G.-H. et al. Electron tunneling through atomically flat and ultrathin hexagonal boron nitride. *Applied Physics Letters* **99**, 243114 (2011).
12. Britnell, L. et al. Field-Effect Tunneling Transistor Based on Vertical Graphene Heterostructures. *Science* **335**, 947 (2012).
13. Song, T. et al. Giant tunneling magnetoresistance in spin-filter van der Waals heterostructures. *Science* **360**, 1214-1218 (2018).
14. Klein, D.R. et al. Probing magnetism in 2D van der Waals crystalline insulators via electron tunneling. *Science* **360**, 1218-1222 (2018).
15. Zhong, D. et al. Van der Waals engineering of ferromagnetic semiconductor heterostructures for spin and valleytronics. *Science Advances* **3**, e1603113 (2017).
16. Jiang, S., Li, L., Wang, Z., Mak, K.F. & Shan, J. Controlling magnetism in 2D CrI₃ by electrostatic doping. *Nature Nanotechnology* **13**, 549-553 (2018).
17. Wang, Z. et al. Tunneling Spin Valves Based on Fe₃GeTe₂/hBN/Fe₃GeTe₂ van der Waals Heterostructures. *Nano Letters* **18**, 4303-4308 (2018).
18. Ralph, D.C. & Stiles, M.D. Spin transfer torques. *Journal of Magnetism and Magnetic Materials* **320**, 1190-1216 (2008).
19. Lee, J.-U. et al. Ising-Type Magnetic Ordering in Atomically Thin FePS₃. *Nano Letters* **16**, 7433-7438 (2016).
20. Fei, Z. et al. Two-dimensional itinerant ferromagnetism in atomically thin Fe₃GeTe₂. *Nature Materials* **17**, 778-782 (2018).
21. Deng, Y. et al. Gate-tunable room-temperature ferromagnetism in two-dimensional Fe₃GeTe₂. *Nature* **563**, 94-99 (2018).
22. Narath, A. Low-Temperature Sublattice Magnetization Of Antiferromagnetic CrCl₃. *Physical Review* **131**, 1929-1942 (1963).
23. Narath, A. & Davis, H.L. Spin-Wave Analysis of the Sublattice Magnetization Behavior of Antiferromagnetic and Ferromagnetic CrCl₃. *Physical Review* **137**, A163-A178 (1965).
24. Kuhlowl, B. Magnetic Ordering in CrCl₃ at the Phase Transition. *Physica Status Solidi (a)* **72**, 161-168 (1982).
25. McGuire, M.A. et al. Magnetic behavior and spin-lattice coupling in cleavable van der Waals layered CrCl₃ crystals. *Physical Review Materials* **1**, 014001 (2017).
26. de Jongh, L.J. & Miedema, A.R. Experiments on simple magnetic model systems. *Advances in Physics* **23**, 1-260 (1974).
27. Mondal, M. et al. Role of the Vortex-Core Energy on the Berezinskii-Kosterlitz-Thouless Transition in Thin Films of NbN. *Physical Review Letters* **107**, 217003 (2011).
28. Kosterlitz, J.M. & Thouless, D.J. Ordering, metastability and phase transitions in two-dimensional systems. *Journal of Physics C: Solid State Physics* **6**, 1181 (1973).
29. Hao, X., Moodera, J.S. & Meservey, R. Thin-film superconductor in an exchange field. *Physical Review Letters* **67**, 1342-1345 (1991).
30. Katmis, F. et al. A high-temperature ferromagnetic topological insulating phase by proximity coupling. *Nature* **533**, 513 (2016).
31. Liu, X., Hsu, H.-C. & Liu, C.-X. In-Plane Magnetization-Induced Quantum Anomalous Hall Effect. *Physical Review Letters* **111**, 086802 (2013).
32. Miron, I.M. et al. Perpendicular switching of a single ferromagnetic layer induced by in-plane current injection. *Nature* **476**, 189 (2011).
33. Pai, C.-F. et al. Spin transfer torque devices utilizing the giant spin Hall effect of tungsten. *Applied Physics Letters* **101**, 122404 (2012).
34. Seyler, K.L. et al. Ligand-field helical luminescence in a 2D ferromagnetic insulator. *Nature Physics* **14**, 277-281 (2018).

35. Miao, G.-X., Müller, M. & Moodera, J.S. Magnetoresistance in Double Spin Filter Tunnel Junctions with Nonmagnetic Electrodes and its Unconventional Bias Dependence. *Physical Review Letters* **102**, 076601 (2009).
36. Wei, P. et al. Strong interfacial exchange field in the graphene/EuS heterostructure. *Nature Materials* **15**, 711 (2016).
37. Klein, D.R. et al. Giant enhancement of interlayer exchange in an ultrathin 2D magnet. arXiv:1903.00002 (2019).
38. Kim, H.H. et al. Evolution of interlayer and intralayer magnetism in three atomically thin chromium trihalides. arXiv:1903.01409 (2019).
39. Wang, L. et al. One-Dimensional Electrical Contact to a Two-Dimensional Material. *Science* **342**, 614 (2013).

Supplementary Materials for

Atomically-Thin CrCl₃: An in-Plane Layered Antiferromagnetic Insulator

Xinghan Cai,^{1,2} Tiancheng Song,¹ Nathan P. Wilson,¹ Genevieve Clark,³ Minhao He,¹ Xiaoou Zhang,⁴ Takashi Taniguchi,⁵ Kenji Watanabe,⁵ Wang Yao,⁶ Di Xiao,⁴ Michael A. McGuire,⁷ David H. Cobden,¹ Xiaodong Xu^{1,3*}

¹Department of Physics, University of Washington, Seattle, Washington 98195, USA.

²National Key Laboratory of Science and Technology on Micro/Nano Fabrication, Department of Micro/Nano Electronics, Shanghai Jiao Tong University, Shanghai 200240, China.

³Department of Materials Science and Engineering, University of Washington, Seattle, Washington 98195, USA.

⁴Department of Physics, Carnegie Mellon University, Pittsburgh, Pennsylvania 15213, USA.

⁵National Institute for Materials Science, Tsukuba, Ibaraki 305-0044, Japan.

⁶Department of Physics and Center of Theoretical and Computational Physics, University of Hong Kong, Hong Kong, China.

⁷Materials Science and Technology Division, Oak Ridge National Laboratory, Oak Ridge, Tennessee 37831, USA.

S1. $I_t - V$ characterization with out-of-plane magnetic field in the bilayer CrCl₃ MTJ.

The tunneling current I_t at selected $\mu_0 H_{out}$ and the extracted sf-TMR ratio as a function of the DC bias voltage are shown in Figures S1a&b, respectively. I_t increases linearly at low bias voltage and exponentially at high bias voltage, which is consistent with Figure 2b. As shown in Figure S1b, the TMR at high $\mu_0 H_{out}$ exhibits oscillating behavior in the low bias regime and becomes negative at large V . This is possibly related to the Landau level formation in the few layer graphite electrodes induced by $\mu_0 H_{out}$, which modulates the carrier density in top and bottom contacts, resulting in a change of the tunneling resistance. Quantitative analysis requires more detailed information about the band structure of CrCl₃ tunnel barrier, and the thickness and doping dependent carrier density in graphite electrodes, which will not be discussed in this work.

S2. Temperature dependent tunneling with out-of-plane magnetic field in the bilayer CrCl₃ MTJ.

Figure S2 exhibits I_t versus T at selected out-of-plane magnetic fields for $V_{ac} = 5$ mV. For small $\mu_0 H_{out}$, I_t first increases with the temperature due to the gradually relaxed interlayer antiferromagnetic coupling of the magnetic moments, followed by a decrease owing to the vanishing intralayer ferromagnetic order, which is consistent with the two-stage magnetic phase transitions with increasing temperature in CrCl₃ as reported in the main text. The critical temperature corresponding to the first transition (antiferromagnetic state to spin polarized state) shifts to the lower temperature side with increasing $\mu_0 H_{out}$ as a result of the competition between the Zeeman energy and the interlayer coupling energy. The critical field ($\mu_0 H_{out}^c = 1.5$ T), at which the magnetic moments get fully polarized at the base temperature, is larger than $\mu_0 H_{in}^c$ (1.2

T) shown in Figures 4a-c, which further confirms the in-plane magnetization of bilayer CrCl₃ as demonstrated in the manuscript.

S3. Bias dependent tunneling in the bilayer CrCl₃ MTJ.

The tunneling current as a function of $\mu_0 H_{in}$ and $\mu_0 H_{out}$ at selected DC bias voltages are displayed in Figures S3a and b, respectively. Both $\mu_0 H_{in}^c$ and $\mu_0 H_{out}^c$ are independent of V in the measured bias voltage range. In the tunneling regime ($V = 5$ mV), the oscillating behavior of I_t at large $\mu_0 H_{out}$ shown with the black curve in Figure S3b is attributed to the quantum oscillations in top and bottom graphite contacts. For $V = 550$ mV, I_t decreases significantly when a large out-of-plane magnetic field is applied, which is possibly related to the Landau level formation and density of states redistribution in graphite electrodes considering that I_t remains almost unchanged at large $\mu_0 H_{in}$.

S4. Effective magnetic phase diagram of the bilayer CrCl₃.

The 2D semi-log plot of dI_t/dT as a function of $\mu_0 H_{in}$ and T of the bilayer CrCl₃ MTJ is shown in Figure S4. dI_t/dT is extracted from Figure 4a. The antiferromagnetic to spin-polarized state and the spin-polarized to paramagnetic state transitions are assigned to occur at the local maximum and minimum in the $dI_t/dT - T$ curves as shown in Figure 4b. In the main text, Figure S4 is replotted as Figure 4c by normalizing each $dI_t/dT - T$ curve by the value of dI_t/dT at its local minimum, in order to exhibit the three distinct magnetic states in a more visualized way.

S5. Electron tunneling through multilayer CrCl₃

We have explored the electron tunneling through multilayer CrCl₃ (more than 3 but less than 10 layers) and show the results of two typical devices in Figures S5a-c and Figures S5d-f respectively. As illustrated in Figures S5a and d, the tunneling is much weaker in both devices compared to the bilayer sample in the main text, but the TMR ratio gets enhanced, owing to the increased CrCl₃ barrier thickness. For the in-plane/out-of-plane magnetic field sweep, while the regular spin canting behavior is observed in the first device (see Figure S5b and S5c), the second device shows an additional dip/kink when sweeping the field across $\mu_0 H_{1in}^c \sim 0.25$ T/ $\mu_0 H_{1out}^c \sim 0.6$ T as shown in Figure. 5e and its inset. Whether these extra features are due to the inhomogeneity of the tunnel barrier is still to be understood, but the fact that $\mu_0 H_{1in}^c$ and $\mu_0 H_{1out}^c$ are close to the critical field at which the ferromagnetic-like spin configuration in bulk CrCl₃ is realized may suggest that some of the multilayer CrCl₃ MTJs recover the properties of the bulk crystal, associated with a dimensional crossover, which is also observed in few layer Fe₃GeTe₂¹ and other ultrathin magnetic systems². Figure S5f shows that this low field feature of I_t exists at all angles between $\mu_0 H_{in}$ and the device. The red curve in the inset's polar plot indicates that at very low field, the tunneling current is slightly anisotropic. This is possibly related to a spin-flop

transition, which has been reported in bulk CrCl_3 ^{3, 4} with an in-plane magnetic field around $\mu_0 H_{\text{flop}} \sim 160$ Oe and will be discussed more in detail in the next section.

S6. Spin-flop transition in multilayer CrCl_3 .

The magnetic anisotropy of the bulk CrCl_3 is weak with the estimated in-plane anisotropy field of only ~ 10 Oe. A spin-flop transition is expected to occur when an in-plane magnetic field is applied parallel to the spins. Experimentally, some signature of the spin-flop has been observed at $\mu_0 H_{\text{in}} = 100 \sim 200$ Oe in CrCl_3 bulk crystals^{3, 4}. However, since the samples used in previous magnetization or magneto-optical measurements usually consist of several CrCl_3 thin flakes with magnetic domains, which are not co-aligned with respect to the same spin orientation, both the spin-flop and the coherent rotation (spin-canting) occur when an in-plane magnetic field is applied, thus any sharp features of the transition are smoothed due to the averaging effect.

In our work, the stacked heterostructure is composed of single crystal CrCl_3 flake and the tunnel junction area is usually less than $\sim 1 \mu\text{m}^2$ to avoid the averaging effect caused by lateral magnetic domain structures. According to the results shown in the main text, no obvious signature of a spin-flop around $\mu_0 H_{\text{in}} \sim 160$ Oe has been observed in our bilayer, trilayer and the first multilayer (Figure S5a-c) CrCl_3 MTJs, implying that the magnetic properties of atomically thin CrCl_3 differ from the bulk crystal. On the other hand, Figure S6 demonstrates a possible spin-flop transition in the second multilayer device (Figure S5d-f) by sweeping $\mu_0 H_{\text{in}}$ at different angles (θ) in the low field regime. At $\theta = 80^\circ$, I_t stays almost unchanged before $\mu_0 H_{\text{in}}$ reaches a critical value, where a sharp jump of I_t occurs, followed by a continuous up-turn upon further increasing $\mu_0 H_{\text{in}}$. This is consistent with the spin-flop transition in a weakly anisotropic antiferromagnetic system, where the magnetization of the material suddenly rotates to the direction perpendicular to the magnetic field that is applied to its easy direction, and then the magnetic moments are gradually aligned by the continuously increasing field. A critical field of $\sim 0.02\text{T}$ here is close to the spin-flop field of the bulk CrCl_3 crystal. When rotating the angle between $\mu_0 H_{\text{in}}$ and the device, the sharp jump of I_t gets smoothed, corresponding to a mixture of the spin-flop and the coherent rotation. As shown in the figure, at $\theta = 160^\circ$, the spin-flop almost disappears and is replaced by a continuous increase of I_t , which is interpreted in terms of the spin-canting effect.

S7. Power dependent photoluminescence (PL) of monolayer CrCl_3

We investigate the insulating nature of the monolayer CrCl_3 by the power dependent PL measurement. Figure S7a shows the optical and atomic force micrograph of typical monolayer CrCl_3 samples. The single broad PL peak around 870 nm characterized using a linearly polarized laser excitation at 2.33 eV with selected powers is illustrated in Figure S7b, which we attribute to a ligand-field transition⁵ and is consistent with the observation shown in Figure 1d in the main text. The PL intensity at 870 nm extracted from Figure S7b is plotted as a function of the laser power in Figure S7c, which can be well fitted with a straight line, indicating that there is no nonlinear effect in the excitation power regime up to 50 μW .

S8. Modelling the tunneling current in the bilayer CrCl₃ MTJ

We use a simple model to fit the magnetic field dependent tunneling current in the bilayer CrCl₃. With a fixed bias voltage, the tunneling current is determined by two factors: the resistance within each layer and the tunneling probability between the two layers. Both of them depend on the directions of the magnetization of the two layers, which can be obtained by minimizing the spin Hamiltonian

$$H = J_{AF} \mathbf{s}_1 \cdot \mathbf{s}_2 + \frac{K}{2} (s_{1,z}^2 + s_{2,z}^2) - g\mu_B \mathbf{B} \cdot (\mathbf{s}_1 + \mathbf{s}_2),$$

where J_{AF} is the interlayer antiferromagnetic exchange energy, K is the easy plane anisotropy energy, and \mathbf{B} is the magnetic field. Here we have assumed that the in-plane ferromagnetic exchange energy is large enough to align all the spins in each layer toward the same direction. The spin in each layer is represented by \mathbf{s}_1 and \mathbf{s}_2 .

Given the magnetization direction, we use a similar method as mentioned in the supplementary material of Ref.⁶ to calculate the tunneling current. Using symmetry analysis, the angular dependent resistance in each layer has the following form

$$\rho(\theta_{Mi}) = \rho_0 + \rho_1 \cos(2\theta_{Mi}),$$

where θ_{Mi} is the angle between the magnetization direction of the i -th layer and the out-of-plane z direction, and the parameters ρ_0, ρ_1 can be determined by fitting the experiment data. Now consider the tunneling probability between the two layers. If the magnetic field is along the z -direction, the tunneling probability is given by Ref. (6)

$$t(\theta_{M1}, \theta_{M2}) = \cos^2 \frac{\theta_{M1} - \theta_{M2}}{2} t_{\parallel} + \sin^2 \frac{\theta_{M1} - \theta_{M2}}{2} t_{\perp},$$

where t_{\parallel}/t_{\perp} is the tunneling probability when the spins in the two layers are parallel/anti-parallel to each other, respectively. Therefore, the tunneling current is

$$\sigma(\theta_{M1}, \theta_{M2}) = \text{const} \times \frac{t(\theta_{M1}, \theta_{M2})}{\rho(\theta_{M1}) + \rho(\theta_{M2})}.$$

If the magnetic field is in-plane, then the magnetization is also in-plane. In this case, we simply regard the direction of the magnetic field as the new z -axis and replace θ_{Mi} with the in-plane polar angle.

We use this model to fit the in-plane and the out-of-plane tunneling current as shown in Figure S8. According to the fitting, the exchange interaction is $J_{AF}S/g\mu_B = 0.6$ T and $KS/g\mu_B = 0.27$ T.

Figures:

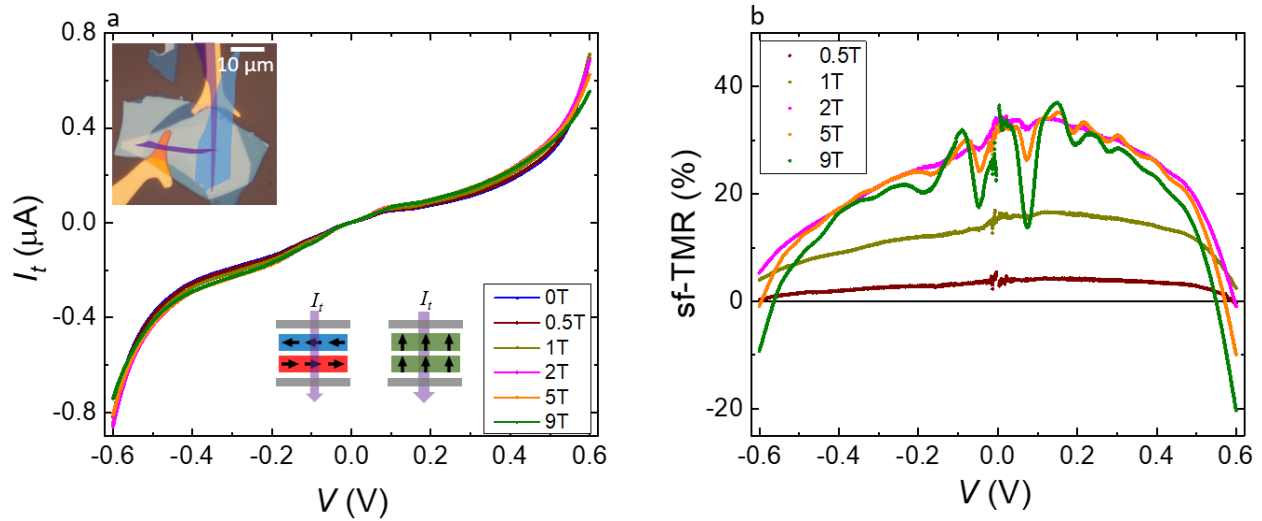


Figure S1. DC transport characterization of a bilayer CrCl_3 sf-MTJ with the out-of-plane magnetic field. (a) Tunneling current as a function of the DC bias voltage at selected out-of-plane magnetic fields. Top left inset: false color optical microscope image of the device. The bottom inset shows the corresponding magnetic states. (b) Extracted sf-TMR ratio as a function of the bias voltage based on (a).

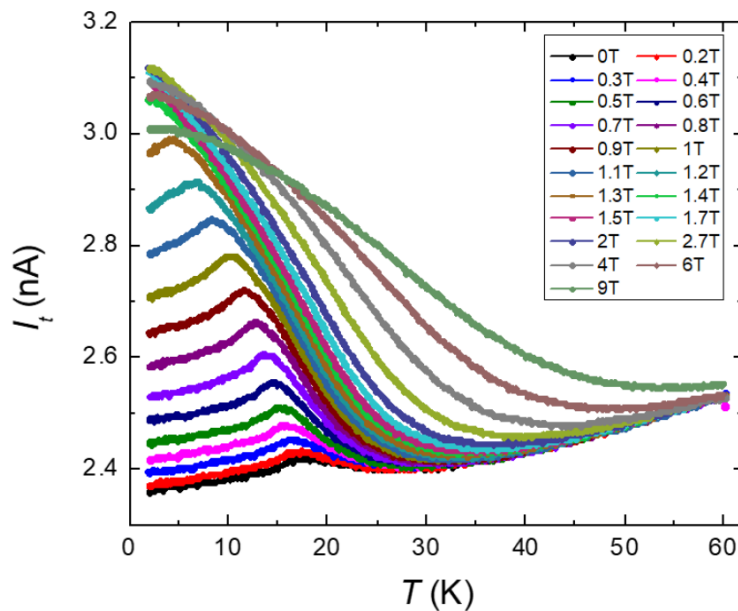


Figure S2. Temperature dependent tunneling of the bilayer CrCl_3 sf-MTJ with the out-of-plane magnetic field. Tunneling current as a function of the temperature at selected out-of-plane magnetic fields with the AC bias voltage $V_{ac} = 5$ mV.

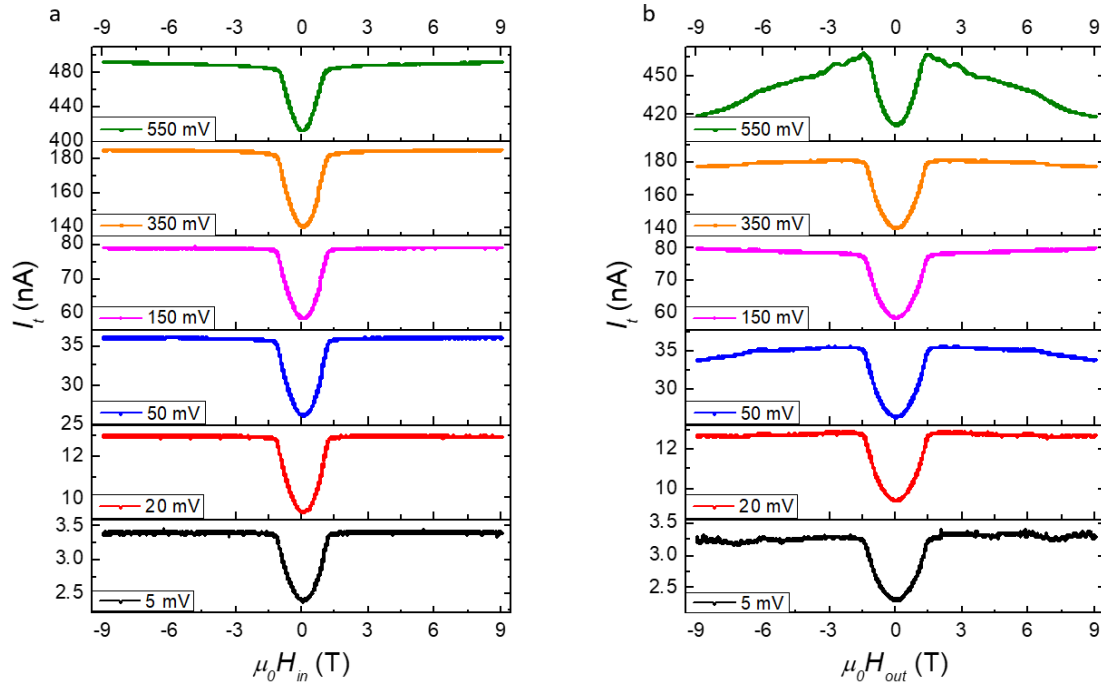


Figure S3. Magnetic field dependent tunneling of the bilayer CrCl_3 sf-MTJ. (a, b) Tunneling current as a function of the in-plane (a) and out-of-plane (b) magnetic field at selected DC bias voltage, respectively.

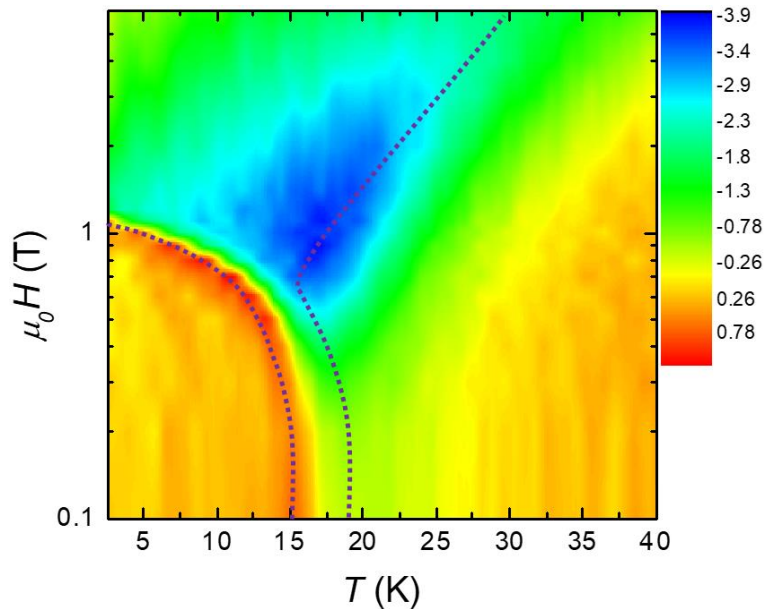


Figure S4. Effective magnetic phase diagram of the bilayer CrCl_3 . 2D semi-log plot of dI_t/dT as a function of the in-plane magnetic field and the temperature. Different magnetic phases are separated by purple dotted lines.

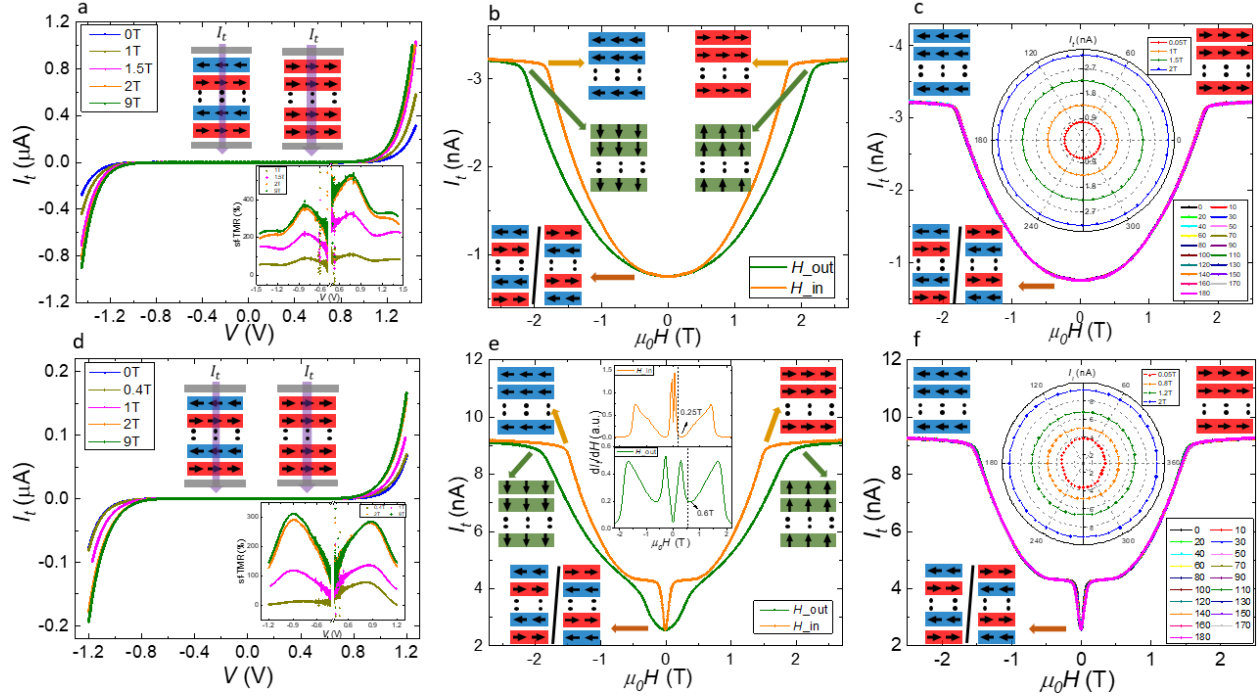


Figure S5. Electron tunneling through multilayer CrCl_3 sf-MTJs. Characterizations on two devices are shown in (a-c) and (d-f) respectively. (a, d) Tunneling current at selected in-plane magnetic fields. Top inset: Schematic of the magnetic configuration for $\mu_0 H_{in} = 0$ T and 9 T. Bottom inset: Extracted sf-TMR ratio as a function of the bias voltage. (b, e) Tunneling current as a function of the in-plane (orange) and out-of-plane (green) magnetic field at selected DC bias voltage $V_{dc} = -900$ mV (b) and $V_{dc} = 900$ mV (e). Insets show the corresponding magnetic states. The top middle inset of (e) shows the derivative of the tunneling current to the in-plane (orange) and out-of-plane (green) magnetic field extracted from (e). (c, f) Tunneling current as a function of the in-plane magnetic field at selected angles θ between the field and the device. $V_{dc} = -900$ mV (c) and $V_{dc} = 900$ mV (f). Insets show the corresponding magnetic states. Top middle inset: Polar plot of $|I_t|$ as a functions of θ at selected magnetic fields. Data points extracted from (c, f).

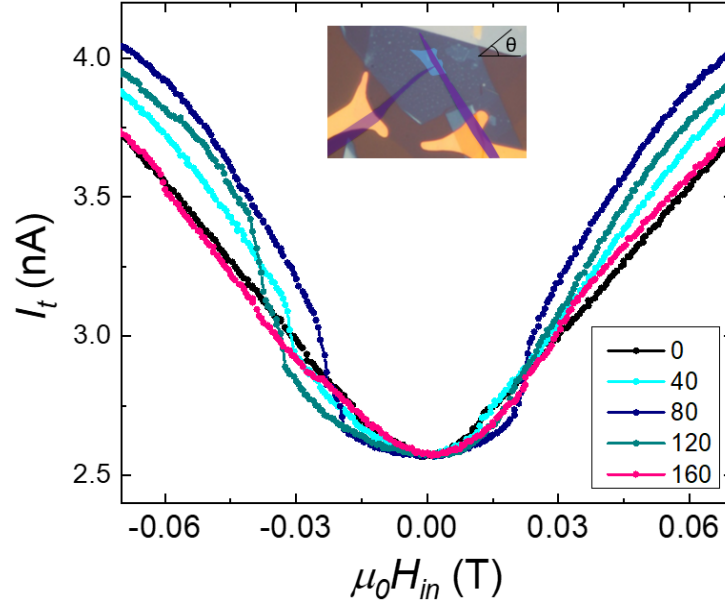


Figure S6. Spin-flop transition in multilayer CrCl_3 . Tunneling current as a function of the in-plane magnetic field at selected angles θ between the field and a multilayer CrCl_3 sf-MTJ. $V_{dc} = 900$ mV. Inset: false color optical microscope image of the device with the defined θ .

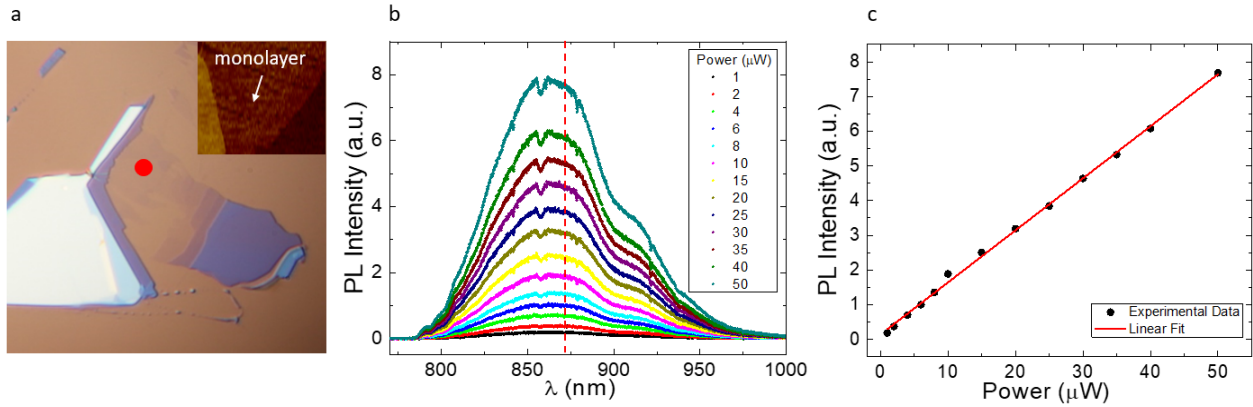


Figure S7. Power dependent PL of monolayer CrCl_3 . (a) Optical microscope image of a CrCl_3 flake. The red spot represents the laser beam spot on the monolayer part. Inset: Atomic force micrograph of another monolayer CrCl_3 flake. (b) PL spectrum from the monolayer CrCl_3 sample shown in (a) with linearly polarized excitation at selected laser powers. The dip in the middle of spectra is due to bad pixels in the CCD. (c) PL intensity at 870 nm as a function of the excitation power. Data points extracted from (b). The red line shows a linear fit to the data.

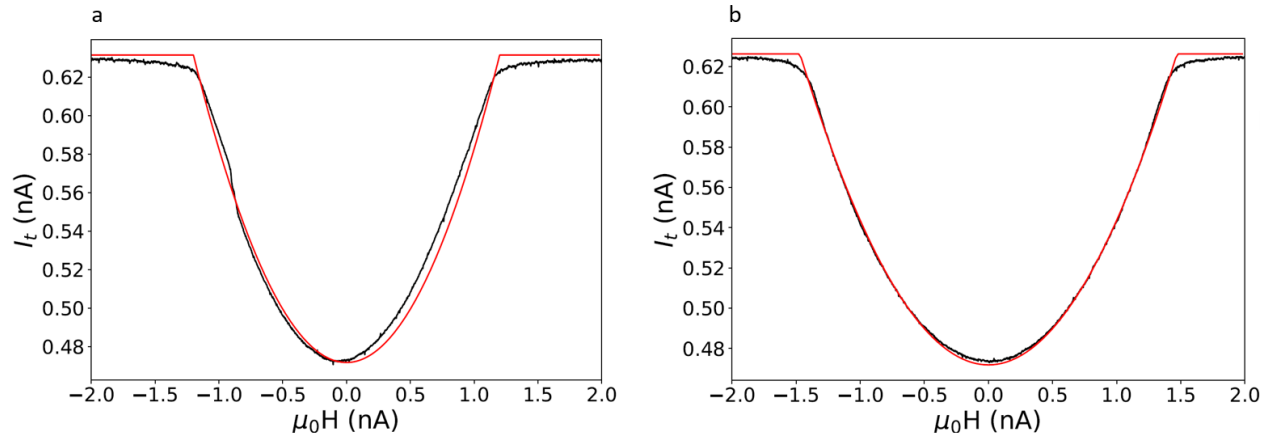


Figure S8. The numerical fitting for the tunneling current under the in-plane (a) and the out-of-plane (b) magnetic field. The red/black curve is the numerical/experimental result, respectively.

REFERENCES

1. Fei, Z. et al. Two-dimensional itinerant ferromagnetism in atomically thin Fe_3GeTe_2 . *Nature Materials* **17**, 778-782 (2018).
2. Li, Y. & Baberschke, K. Dimensional crossover in ultrathin Ni(111) films on W(110). *Physical Review Letters* **68**, 1208-1211 (1992).
3. Kuhlow, B. Magnetic Ordering in CrCl_3 at the Phase Transition. *Physica Status Solidi (a)* **72**, 161-168 (1982).
4. McGuire, M.A. et al. Magnetic behavior and spin-lattice coupling in cleavable van der Waals layered CrCl_3 crystals. *Physical Review Materials* **1**, 014001 (2017).
5. Seyler, K.L. et al. Ligand-field helical luminescence in a 2D ferromagnetic insulator. *Nature Physics* **14**, 277-281 (2018).
6. Song, T. et al. Giant tunneling magnetoresistance in spin-filter van der Waals heterostructures. *Science* **360**, 1214-1218 (2018).